

# Asymmetric second-order coherence function in atomic arrays

Nikita Nefedkin<sup>1</sup> and Andrea Alù<sup>1, 2</sup>

<sup>1</sup>*Photonics Initiative, Advanced Science Research Center,  
City University of New York, New York, NY 10031, USA\**

<sup>2</sup>*Physics Program, Graduate Center, City University of New York, New York, NY 10016, USA<sup>†</sup>*

Collective effects in atomic arrays provide unique opportunities for controlling light-matter interactions, with potential applications in quantum information processing and photonic technologies. In this work, we investigate the emission characteristics of small,  $N < 10$ , arrays of two-level atoms in free space, focusing on how the direction of an incident electromagnetic wave affects the collective or individual emission properties. By examining photon emission statistics, we show that collective emission can be selectively excited based on the direction of the incident field, highlighting a tunable asymmetry in the emission properties. This directional control over the collective response is achieved through adjustments in system parameters, such as array geometry, atomic spin orientation and transition frequency, enabling us to manipulate both the angular distribution and statistical properties of the emitted light. Our findings contribute to the broader understanding of collective effects in atomic systems and open new pathways for engineering direction-sensitive quantum light sources with tailored angular-dependent emission statistics and intensity.

## INTRODUCTION

The transition from isolated quantum entities to complex many-body systems has opened the door to creating macroscopic quantum states with highly controllable properties [1–5]. Many-body quantum systems, consisting of multiple interacting particles, can exhibit collective behaviors that are fundamentally distinct from those of individual particles [3, 6, 7], enabling novel states of light and matter that transcend traditional, single-particle quantum phenomena. These collective states are of particular interest for advancing quantum information processing, where harnessing the correlated behavior of large ensembles can significantly enhance performance and scalability [8–10]. Utilizing collective effects in such systems, including phenomena like superradiance and subradiance [11–14], offers powerful new ways to control light-matter interactions and explore quantum coherence on a macroscopic scale.

For example, superradiance and subradiance describe two distinct regimes of collective emission in atomic systems. In superradiance, the presence of cooperative interactions among atoms amplifies the emission, leading to a burst of radiation that is faster and more intense than the sum of individual emissions [12, 15]. Conversely, subradiance results in suppressed emission due to destructive interference between atoms, effectively trapping light within the system. Switching between a superradiant or subradiant state and a non-collective state provides a versatile mechanism for modulating emission rates and the system's coherence properties, critical for applications requiring controlled photon sources or quantum state preservation.

For practical applications in quantum optics and information processing, controlling the statistical properties of emission from atomic systems is essential [16]. Emission statistics, particularly second-order correlation

functions  $g^{(2)}(\tau)$ , offer insight into the temporal correlations and coherence of emitted photons, which are crucial for developing deterministic single-photon sources [17], entangled photon pairs [18], and other quantum light sources [19]. Controlling these statistical properties in collective atomic arrays can lead to new methods for tuning photon emission, opening avenues for enhanced quantum communication protocols and scalable quantum networks.

A potential approach to controlling emission statistics lies in the concept of asymmetric response to the external perturbation, analogous to nonreciprocity [20–24]. By carefully selecting system parameters and the direction of excitation, it is possible to introduce an asymmetry in the system state excitation, i.e., trapping the system in a slowly decaying collective state for one direction and leaving it primarily in the ground state for another direction [23–25], which leads to the asymmetry in the emission statistics as well. This approach enables directional control over collective and individual emissions, allowing selective excitation of collective states based on the direction of incident electromagnetic (EM) waves. Such asymmetric emission can enhance the versatility of quantum light sources by offering new degrees of freedom in emission control without the need for complex waveguides or cavity structures. This capability is particularly valuable for atomic systems, such as cold atom ensembles in optical lattices and trapped ions.

In this work, we study the emission from arrays of two-level atoms, focusing on how the direction of the incident EM wave influences collective and individual emission characteristics. We investigate the photon emission statistics, including the angular dependence of the second-order coherence function, as a function of excitation direction. This highlights the emergence of collective emission phenomena and methods to distinguish collective behavior from individual atomic emissions. Our ap-

proach provides insight into controlling emission properties in free-space atomic arrays, contributing to the broader goal of engineering robust, direction-sensitive quantum light sources with tunable coherence and emission dynamics.

### ATOMIC CHAIN INTERACTING WITH THE INCIDENT EM WAVE

We start from the general consideration of a system of atoms aligned in a chain. Let us consider  $N$  two-level atoms located along the  $z$  axis with a period  $a$ . For simplicity, we assume that all atoms have the same dipole moment  $\mathbf{d} = d\mathbf{e}_x$ , oriented along  $x$  axis, see Fig. 1. We denote  $|g_j\rangle$  and  $|e_j\rangle$  the ground and excited states of the  $j$ th atom,  $j = 1, \dots, N$ . The transition rate between these states we denote as  $\omega_j$ . Each atom, considered single in free space, spontaneously emits with rate  $\gamma_0^j = \frac{\omega_j^3 d^2}{3\pi\epsilon_0\hbar c^3}$  [26], where  $\epsilon_0$  is the vacuum permittivity and  $c$  is the speed of light. For simplicity of notation, we normalize the decay rates of atomic collective modes by the spontaneous emission rate of a single atom in free space.

To excite the atom chain, we consider a monochromatic EM plane wave. For simplicity, we consider these waves to propagate along the  $z$  axis, i.e. along the array of atoms. Of course, it is straightforward to generalize the consideration to tilted excitation directions. The incident electric field is  $\mathbf{E}_{in}(\mathbf{r})e^{-i\omega_0 t} = E_0 \mathbf{e}_x e^{i\mathbf{k}_0 \cdot \mathbf{r}} e^{-i\omega_0 t}$ , where the wave vector  $\mathbf{k}_0 = \pm k_0 \mathbf{e}_z$  has absolute value  $k_0$  and points towards either the  $+z$  or  $-z$  direction. For brevity, we define as *forward*  $+z$  direction and as *backward*  $-z$  direction, see Fig. 1.

The full description of the system depicted in Fig. 1 includes taking into account the continuum of EM modes of free space, all the degrees of freedom of the atoms, and the interaction between the EM modes and atoms. This approach turns out to be challenging, even when it comes to finding an approximate numeric solution. Therefore, we follow the standard procedure [26–28] of eliminating the field degrees of freedom, considering them as a thermal reservoir with a temperature close to zero. This is possible by applying the Born-Markov approximation. Assuming that the relaxation time of the atoms is much slower than the relaxation time of the photonic reservoir and the time required by light to propagate between atoms, the photonic degrees of freedom can be traced out from the full Hamiltonian of the system, resulting in an effective master equation which involves only atomic degrees of freedom. Quantitatively, the Born-Markov approximation requires the  $\gamma_{max}^{-1} \gg a_{max}/c$ , where  $\gamma_{max}$  is the largest atomic decay rate, and  $a_{max}$  is the largest inter-atomic distance in the array. The effective master

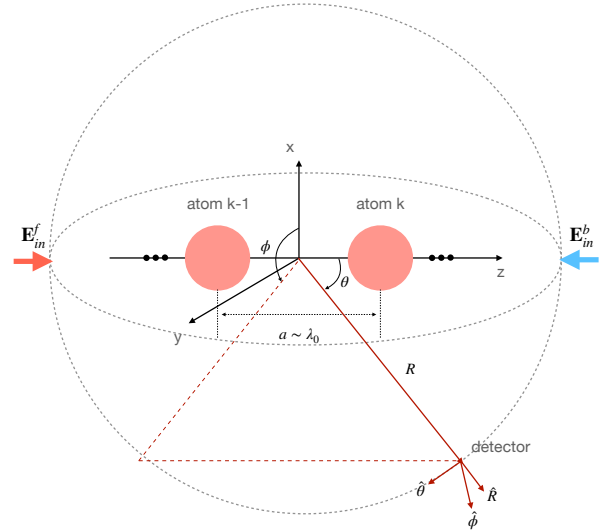


FIG. 1: Chain of two-level atoms interacting with incident EM waves propagating in  $+z$  (forward) direction and  $-z$  (backward) direction. Detectors register the emission from the array in the far field zone; the positions of the detectors are written in spherical coordinates.

equation reads as follows:

$$\dot{\hat{\rho}} = \frac{i}{\hbar} [\hat{\rho}, \hat{H}_S] + \sum_{i,j=1}^N \frac{\Gamma_{ij}}{2} (2\hat{\sigma}_j \hat{\rho} \hat{\sigma}_i^\dagger - \hat{\rho} \hat{\sigma}_i^\dagger \hat{\sigma}_j - \hat{\sigma}_i^\dagger \hat{\sigma}_j \hat{\rho}). \quad (1)$$

Here the lowering and raising operators  $\hat{\sigma}_j = \underbrace{\hat{I} \otimes \dots \otimes \hat{\sigma}_j \otimes \dots \otimes \hat{I}}_{j-1} \otimes \dots \otimes \underbrace{\hat{\sigma}_j^\dagger \otimes \dots \otimes \hat{I}}_{N-j}$  and  $\hat{\sigma}_j^\dagger = \underbrace{\hat{I} \otimes \dots \otimes \hat{\sigma}_j^\dagger \otimes \dots \otimes \hat{I}}_{j-1} \otimes \dots \otimes \underbrace{\hat{I} \otimes \dots \otimes \hat{\sigma}_j \otimes \dots \otimes \hat{I}}_{N-j}$  describe the relaxation and excitation of the  $j$ th atom, where  $\hat{\sigma} = |g\rangle\langle e|$  and  $\hat{\sigma}^\dagger = |e\rangle\langle g|$  are transition operators between excited  $|e\rangle$  and ground  $|g\rangle$  states;  $\hat{I}$  is the identity operator. Note that here, we assumed that the thermal excitations in the reservoir are negligible due to its close to zero temperature, and thus, dissipation takes place only from the atomic system to the reservoir and not vice versa. For an ensemble of atoms arbitrarily arranged with regard to restrictions of the Born-Markov approximation, the effective Hamiltonian of the system in the rotating frame with the frequency of the incident EM field  $\omega_0$  is [8, 27, 29]

$$\begin{aligned} \hat{H}_S = \hbar \sum_{k=1}^N & \left( \frac{\Delta_k}{2} \hat{\sigma}_z^k - \Omega_R^k \hat{\sigma}_k - \Omega_R^{k*} \hat{\sigma}_k^\dagger \right) + \\ & \hbar \sum_{i \neq j}^N \Omega_{ij} \hat{\sigma}_i^\dagger \hat{\sigma}_j, \end{aligned} \quad (2)$$

where the indices  $k, i, j$  run over all the atoms and  $\hat{\sigma}_z^k = [\hat{\sigma}_k^+, \hat{\sigma}_k^-]$  stands for the population inversion of the  $k$ th atom. The detuning between the  $k$ th atom and the incident field we define as  $\Delta_k = \omega_k - \omega_0$ , and the interaction constant between the incident field and the  $k$ th atom,  $\Omega_R^k = \mathbf{d} \cdot \mathbf{E}_{\text{in}}^+(\mathbf{r}_k)/\hbar$ . For a fixed dipole moment of the atomic transition and the fixed position of the atom, the interaction constant is proportional to the incident field amplitude in the coordinate of the atom. The effective dipole-dipole interaction arises in the system due to the interaction of the atoms with the EM modes of free space. The constant of the dipole-dipole interaction between  $j$ th and  $k$ th atoms takes the form:

$$\begin{aligned} \mathcal{H}_{jk} &= -\frac{3\pi c}{\omega} \sqrt{\gamma_0^j \gamma_0^k} \mathbf{d}_j^* \bar{\mathbf{G}}(\mathbf{r}_j, \mathbf{r}_k, \omega) \mathbf{d}_k \\ &= \Omega_{jk} - \frac{i}{2} \Gamma_{jk} \end{aligned} \quad (3)$$

where the real part is responsible for coherent interactions, and the imaginary part is responsible for dissipative interactions. In eq. (3),  $\bar{\mathbf{G}}$  is the free-space Green's tensor that reads

$$\bar{\mathbf{G}}(\mathbf{r}, \mathbf{r}', k) = \left[ \bar{\mathbf{I}} + \frac{1}{k^2} \nabla \nabla \right] \frac{e^{ik|\mathbf{r}-\mathbf{r}'|}}{4\pi |\mathbf{r} - \mathbf{r}'|} \quad (4)$$

and  $\bar{\mathbf{I}}$  is a unit tensor of the second order.

In this work, we focus on the statistical properties of the atomic array emission. The key characteristic reflecting the statistical nature of the emission from the array is the second-order coherence function defined as follows [16]:

$$\begin{aligned} g^{(2)}(\mathbf{R}_1, t_1; \mathbf{R}_2, t_2) &= \\ &\frac{\langle \hat{\mathbf{E}}_{\text{sc}}^{(-)}(\mathbf{R}_1, t_1) \hat{\mathbf{E}}_{\text{sc}}^{(-)}(\mathbf{R}_2, t_2) \hat{\mathbf{E}}_{\text{sc}}^{(+)}(\mathbf{R}_2, t_2) \hat{\mathbf{E}}_{\text{sc}}^{(+)}(\mathbf{R}_1, t_1) \rangle}{\langle \hat{\mathbf{E}}_{\text{sc}}^{(-)}(\mathbf{R}_1, t_1) \hat{\mathbf{E}}_{\text{sc}}^{(+)}(\mathbf{R}_1, t_1) \rangle \langle \hat{\mathbf{E}}_{\text{sc}}^{(-)}(\mathbf{R}_2, t_2) \hat{\mathbf{E}}_{\text{sc}}^{(+)}(\mathbf{R}_2, t_2) \rangle} \end{aligned} \quad (5)$$

This is the  $g^{(2)}$  function for the field scattered from the atom array, which operator is given by:

$$\hat{\mathbf{E}}_{\text{sc}}^+(\mathbf{r}) = \frac{\omega^2}{\epsilon_0 c^2} \sum_{j=1}^N \bar{\mathbf{G}}(\mathbf{r}, \mathbf{r}_j, \omega) \mathbf{d}_j \hat{\sigma}_j \quad (6)$$

In the further sections, we will consider the way of calculating the second-order coherence function, eq. (5).

## COLLECTIVE STATES IN THE ENSEMBLE OF ATOMS

Understanding the collective behavior of atomic ensembles is essential for exploring the full range of quantum phenomena that arise from interactions between light and matter in many-body systems. When multiple atoms are arranged in close proximity — particularly within subwavelength distances — their individual

responses to light become highly correlated, leading to emergent phenomena that do not manifest in isolated atoms. These collective effects can give rise to unique quantum states and dynamical properties, such as subradiance, superradiance [12–14], and nonreciprocal behavior [23, 30, 31], which are of considerable interest in both fundamental research and potential applications in quantum information and communication.

The many-body system consisting of  $N$  atoms allows for the existence of the collective states, which significantly modify its dynamics. Examples of these collective states are subradiant (or dark) states and superradiant (or bright) states. A slower decay rate than the decay rate of the individual atom in the array characterizes the subradiant state. It has the form of a fully antisymmetric state with regard to atoms' permutations [12]. In the case of an ensemble of atoms located in a subwavelength volume, the decay rate from the subradiant state is equal to zero. The superradiant state, on the other hand, is the state with the fastest decay rate, proportional to  $N^2$  if the atoms are located in the subwavelength volume, and it has the form of a fully symmetric state with regard to permutations of the atoms [12].

For the system depicted in Fig. 1, the subradiant and superradiant states may be obtained by diagonalizing the effective non-Hermitian Hamiltonian:

$$\hat{H}_{\text{eff}} = \hat{H}_S - i\hbar \sum_{j,k} \frac{\Gamma_{jk}}{2} \hat{\sigma}_j^+ \hat{\sigma}_k^- \quad (7)$$

where the imaginary part accounts for dissipation. However, in the general case, where  $\omega_j \neq \omega_k$  and consequently  $\gamma_0^j \neq \gamma_0^k$ ,  $k \neq j$ ,  $k, j = 1, \dots, N$ , it is difficult to diagonalize the Hamiltonian in eq. (7). Thus, to demonstrate the existence of the dark,  $|D\rangle$ , and bright,  $|B\rangle$ , states, we consider the system of two identical atoms in resonance with the incident field,  $\omega_1 = \omega_2 = \omega_0$ . In this case, we can find the dark and bright states by diagonalizing only the dissipative part of the Hamiltonian (7), which is equivalent to diagonalizing the matrix  $(\Gamma_{jk})$  [12, 32, 33]. Its eigenvalues give the decay rates of the collective states in the system, namely,  $|D\rangle$  and  $|B\rangle$ . To obtain the form of these states, one needs to act by a corresponding collective operator on the system's ground state,  $|G\rangle$  [32, 33].

In the more general case of  $N$  atoms, this procedure can be formalised in the following way. The collective operators or the source-mode jump operators have the form:

$$\vec{J} = \sqrt{\Lambda} \mathbf{B} \vec{\Sigma} \quad (8)$$

$$\vec{J}^\dagger = \vec{\Sigma}^\dagger \mathbf{B}^T \sqrt{\Lambda}, \quad (9)$$

where

$$(\Gamma_{jk}) = \mathbf{B}^T \Lambda \mathbf{B}, \quad \Lambda = \text{diag}(\lambda_1, \dots, \lambda_N) \quad (10)$$

$$\vec{\Sigma} = (\hat{\sigma}_1, \dots, \hat{\sigma}_N) \quad (11)$$

The dissipative part of the master equation (1) rewrites in terms of collective operators (8), (9) as follows:

$$\mathcal{D}_J(\cdot) = \frac{1}{2} \sum_{m=1}^N \left( 2\hat{J}_m \cdot \hat{J}_m^\dagger - \hat{J}_m^\dagger \hat{J}_m - \hat{J}_m \cdot \hat{J}_m^\dagger \right), \quad (12)$$

where operators  $\hat{J}_m$  are source-mode jump operators that produce the photons with rate  $\lambda_m$ . These operators are the elements of the vector (8).

In the case of two atoms in the array, the dark and bright states decay rates are  $\gamma_B = \gamma_0 + \Gamma_{12}$  and  $\gamma_D = \gamma_0 - \Gamma_{12}$ . We assumed identical atoms here, so  $\Gamma_{11} = \Gamma_{22} = \gamma_0$ . If we substitute  $\Gamma_{12}$  using formula (3), we obtain the following expression for the decay rates of  $|D\rangle$  and  $|B\rangle$ :

$$\frac{\gamma_{D/B}}{\gamma_0} = 1 \mp \frac{3 |k_0 a \cos(k_0 a) + (k_0^2 a^2 - 1) \sin(k_0 a)|}{2k_0^3 a^3} \quad (13)$$

where  $k_0 = \omega_0/c$ . Note that  $\gamma_B = 2\gamma_0$  and  $\gamma_D = 0$  in the case of a subwavelength array,  $a \rightarrow 0$ , and these decay rates respond to the decay rates of conventional superradiant and subradiant states [11, 13, 34, 35]. By applying the collective operators corresponding to  $|D\rangle$  and  $|B\rangle$  states to the ground state, we obtain these states on the uncoupled basis:

$$|D\rangle = \frac{1}{\sqrt{2}} (|e, g\rangle - |g, e\rangle) \quad (14)$$

$$|B\rangle = \frac{1}{\sqrt{2}} (|e, g\rangle + |g, e\rangle) \quad (15)$$

As shown before [10, 23–25], the collective states play the pivotal role in nonreciprocity effects in atomic arrays. Excitation of the system with an EM wave from one direction populates the dark collective state, whereas excitation from the other direction remains in the ground state. This asymmetry in the system's state populations leads to nonreciprocal behaviour of the light scattered by the system, i.e., in the general case to nonreciprocal total extinction cross section [31]. In this work, we utilize the idea of populating system states asymmetrically for different excitation directions to explore how the statistical properties of the emission change under these conditions.

## SECOND-ORDER COHERENCE FUNCTION FOR DIRECTED-DETECTION OPERATORS

Let us examine the expression for the second-order coherence function  $g^{(2)}$ , as defined in equation (5). This expression quantifies the degree of coherence of the field scattered from the atomic array at two distinct points in space and time. Physically, it is interpreted as the correlation between the signals from two detectors positioned at points  $\mathbf{R}_1$  and  $\mathbf{R}_2$ , measuring the intensity of the scattered field,  $\langle |\hat{\mathbf{E}}_{sc}^+(\mathbf{r}, t)|^2 \rangle$ , from the array at times  $t_1$  and  $t_2$ .

The expression in equation (6) is the operator of the scattered field, which depends explicitly on the dyadic Green tensor of the environment and encompasses a summation over all atoms in the array. Computing the correlation functions within the  $g^{(2)}$  function can be challenging in this form. To simplify our analysis, we restrict ourselves to the far-field approximation, where the detectors are situated much farther from the array than the wavelength of the scattered field and the geometric size of the array, i.e.,  $|\mathbf{R}_j| \gg \lambda_0, Na$ , where  $j$  is the index of the detector.

To account for photons emitted in a specific direction  $\bar{\mathbf{R}}(\theta, \varphi) = \mathbf{R}/R$ , where  $\mathbf{R}$  is the detector's coordinate and  $R = |\mathbf{R}|$  (see Fig. 1), and detected within the solid angle element  $d\Omega$  in the far field, we follow Ref. [32] and introduce the directional collective operators:

$$\hat{S}(\theta, \varphi) = \sqrt{\frac{2\epsilon_0 c}{\hbar\omega_0}} (R^2 d\Omega) \hat{E}_{sc}^+(\mathbf{R}(\theta, \varphi), t), \quad (16)$$

where the operator of the scattered field in the far field takes the form:

$$\hat{E}_{sc}^+(\mathbf{r}, t) = \frac{3\hbar\gamma_0}{4dk_0} \frac{\sqrt{1 - (\bar{\mathbf{d}} \cdot \bar{\mathbf{r}})^2}}{|\mathbf{r}|} \sum_{j=1}^N e^{-ik_0 \bar{\mathbf{r}} \cdot \mathbf{r}_j} \hat{\sigma}_j(t), \quad (17)$$

$$\bar{\mathbf{d}} = \frac{\mathbf{d}}{d}, \quad \bar{\mathbf{r}} = \frac{\mathbf{r}}{|\mathbf{r}|}$$

and  $\mathbf{r}_j$  denotes the coordinate of the  $j$ -th atom. By substituting equation (17) into equation (16) and transitioning to spherical coordinates, we arrive at the simplified form of the directional collective operator:

$$\hat{S}(\theta, \varphi) = \sqrt{\gamma_0 D(\theta, \varphi) d\Omega} \sum_{j=1}^N e^{-ik_0 \bar{\mathbf{r}}(\theta, \varphi) \cdot \mathbf{r}_j} \hat{\sigma}_j, \quad (18)$$

where

$$D(\theta, \varphi) = \frac{3}{8\pi} \left[ 1 - (\bar{\mathbf{d}} \cdot \bar{\mathbf{r}}(\theta, \varphi))^2 \right] \quad (19)$$

is the dipole radiation pattern for emission from an individual atom.

Notably, the dissipative part of the master equation (1) can be expressed in terms of the directional collective operators (18), which provides a clear physical interpretation of detecting scattered photons emitted by the atomic array in the direction  $(\theta, \varphi)$ . Thus, the dissipative part takes the following form:

$$\begin{aligned} \mathcal{D}_S(\cdot) = \frac{1}{2} \int d\Omega & \left( 2\hat{S}(\theta, \varphi) \cdot \hat{S}^\dagger(\theta, \varphi) - \right. \\ & \left. \hat{S}^\dagger(\theta, \varphi) \hat{S}(\theta, \varphi) - \hat{S}^\dagger(\theta, \varphi) \hat{S}(\theta, \varphi) \right) \end{aligned} \quad (20)$$

We can now rewrite the  $g^{(2)}$  function in terms of the operators  $\hat{S}(\theta, \varphi)$ . It takes the form:

$$g^{(2)}(0) = \frac{\langle \hat{S}^\dagger(\theta, \varphi) \hat{S}^\dagger(\theta, \varphi) \hat{S}(\theta, \varphi) \hat{S}(\theta, \varphi) \rangle}{\langle \hat{S}^\dagger(\theta, \varphi) \hat{S}(\theta, \varphi) \rangle^2} \quad (21)$$

We can compute the second-order coherence function in the far field from this equation, depending on the angles  $\theta$  and  $\varphi$ . Due to the axial symmetry of the system along the  $z$ -axis (see Fig. 1), we can focus solely on the  $\theta$  dependence of the  $g^{(2)}(0)$  function at a fixed  $\varphi$  angle.

To compute the coherence function, following Ref. [31], we choose such system parameters that optimize *nonreciprocal extinction efficiency* (see [31] for details) given by formula:

$$\mathcal{M} = \max \left( \sigma_{\text{tot}}^f, \sigma_{\text{tot}}^b \right) \left| \frac{\sigma_{\text{tot}}^f - \sigma_{\text{tot}}^b}{\sigma_{\text{tot}}^f + \sigma_{\text{tot}}^b} \right| \quad (22)$$

where  $\sigma_{\text{tot}}^{f/b}$  is total extinction cross section for forward ( $f$ ) or backward ( $b$ ) excitation having the following expression:

$$\sigma_{\text{tot}}(\mathbf{k}_0) = \frac{4\pi}{k_0} \text{Im} (\mathbf{e}_0^* \cdot \mathbf{f}(\mathbf{k} = \mathbf{k}_0)) \quad (23)$$

where  $\mathbf{e}_0$  is the polarization of the incident field and  $\mathbf{f}(\mathbf{k})$  is the scattering amplitude along the direction defined by  $\mathbf{k}$  [36].

Choosing the system parameters in such a way, we make sure that the most populated state for one of the directions of excitation is the dark state [eq. (14) in a case of two atoms], indicating that the system is in a collective state. Thus, we calculate the radiation pattern of the emission (i.e., the number of emitted photons as a function of the angles) and the angular distribution of the coherence function (21) for parameters that maximize the population of the collective state. Figure 2 illustrates the angular dependence of the  $g^{(2)}(0)$  function alongside the emission intensity.

The direction of excitation strongly influences the system's behavior, including the scattering dynamics and the statistical properties. The asymmetry in emission properties is evident in the contrast between forward ( $+z$ ) and backward ( $-z$ ) excitation directions, as shown in the angular dependence of the emission patterns and  $g^{(2)}(0)$  for different numbers of atoms (e.g.,  $N = 2$  and  $N = 4$ ). When the system is excited from the backward direction in the two-atom array (Fig. 2a,c), the emission intensity is strongly enhanced, and photon bunching is observed in the directions perpendicular to the array and antibunching – in the direction along the arrays. For this direction of excitation, the system dominantly occupies the collective dark state  $|D\rangle$ , which decays slowly. In contrast, forward excitation primarily results in antibunching behavior for the transmitted light and bunching for the reflected light. The  $g^{(2)}(0)$  function is oriented along the array.

In the four-atom chain (Fig. 2b,d), when the system is excited in the forward direction, the emitted light shows an enhanced intensity in  $+z$  direction, with the  $g^{(2)}(0)$  function indicating bunching behavior for the reflected light,  $-z$  direction. Conversely, for backward excitation,

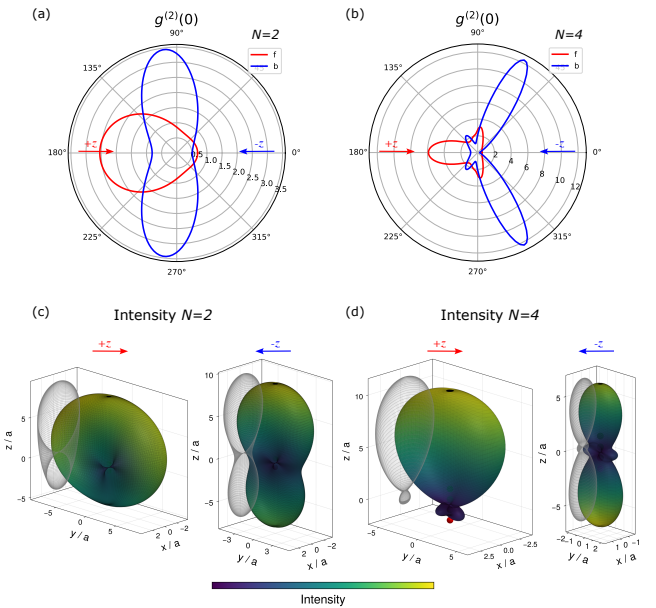


FIG. 2: Angular distribution of the second-order coherence function,  $g^{(2)}(0)$ , when the system is primarily in the dark state for the two-atom chain (a) and for the four-atom chain (b) for the forward and backward excitation directions, along with the radiation patterns corresponding to the parameters used for the  $g^{(2)}(0)$  function computations (c-d). The parameters optimizing the total scattering cross section are as follows: (a), (c)  $a = \lambda_0/4$ ,  $|\Omega_R| = 0.3\gamma_0$ ,  $\Delta_2 = -\Delta_1 = 0.3\gamma_0$ ; (b), (d)  $a = \lambda_0/5$ ,  $|\Omega_R| = 0.13\gamma_0$ ,  $\Delta_4 = \Delta_3 = -\Delta_2 = -\Delta_1 = 0.43\gamma_0$ , where  $\lambda_0$  is the wavelength of the incident EM wave.

the emission shows a different spatial intensity profile and reduced photon correlations in the direction along the array, as seen in the  $g^{(2)}(0)$  function. Here, the tendency toward antibunching is more prominent. This shift in behavior between forward and backward excitation illustrates how the emission pattern and photon statistics vary significantly with the direction of the incident EM wave in the four-atom array.

Thus, by selecting the detector's position and tuning the excitation direction, one can effectively manipulate the statistical character of the emitted light, transitioning between bunching and antibunching behavior. Such control over the emission pattern and statistics has potential applications in tailoring the quantum properties of light emitted from atomic arrays, allowing for precise tuning of coherence and correlation characteristics based on external excitation conditions.

Ultimately, the capability to control emission statistics on demand is closely linked to the occupation of collective states, particularly the slowly decaying dark state  $|D\rangle$ . This allows us to identify the state exhibiting the slowest

decay rate, providing insights into the system's response under various excitation conditions. To deepen our understanding of the system's evolution as we vary the excitation direction, we turn to the formalism of quantum trajectories, as described in the works [32, 33, 37]. This approach enables us to unravel the dynamics governed by the master equation (1), offering a comprehensive view of how the system evolves in response to different excitation scenarios.

### COLLECTIVE JUMP OPERATORS AND WAITING TIME DISTRIBUTIONS

Following Carmichael's works [32, 33, 37], we can expand the reduced density operator of the system as a series of scattering records, i.e., the sequence of detection events that track a quantum system's interaction with its environment, as

$$\hat{\rho}(t) = \sum_{rec} P(rec) |\psi_c(t)\rangle\langle\psi_c(t)|,$$

where  $rec$  is the record denoting a particular sequence of photon detections (emissions) up to time  $t$ , the state  $|\psi_c(t)\rangle = |\bar{\psi}_c(t)\rangle/\sqrt{\langle\bar{\psi}_c(t)|\bar{\psi}_c(t)\rangle}$  is the normalized state of the atoms conditioned on the occurrence of the sequence  $rec$ , and  $\bar{\psi}_c(t)$  is an unnormalized state of the atoms conditioned on  $rec$ . The probability  $P(rec) = \langle\bar{\psi}_c(t)|\bar{\psi}_c(t)\rangle$  corresponds to a particular scattering record, satisfying  $\sum_{rec} P(rec) = 1$ . As shown in Ref. [32], we can construct such  $|\psi_c(t)\rangle$  that the expansion holds with  $\hat{\rho}(t)$  satisfying the master equation (1), and  $P(rec)$  gives the correct frequency of occurrence for every conceivable record.

The time evolution of  $|\bar{\psi}_c(t)\rangle$  is generated by an effective non-Hermitian Hamiltonian:

$$\hat{H}_{\text{eff}} = \hat{H}_S - i\hbar \sum_j \hat{O}_j^\dagger \hat{O}_j, \quad (24)$$

and is punctuated by jumps generated by a set of jump operators  $\hat{O}_j$  at the times of photon emissions. In our case, the jump operators may be directed-detection operators  $\hat{S}(\theta, \varphi)$  (18) or the source-mode operators  $\hat{J}_m$ . The evolution follows the non-unitary Schrödinger equation with Hamiltonian  $\hat{H}_{\text{eff}}$ .

This time evolution can be simulated using the Monte Carlo method, as described in Ref. [37]. Formally, the unnormalized state  $|\bar{\psi}_c(t)\rangle$  for  $n$  recorded events can be written as:

$$|\bar{\psi}_c(t)\rangle = \hat{B}(t - t_n) \hat{O}_n \hat{B}(t_n - t_{n-1}) \times \hat{O}_{n-1} \dots \hat{O}_1 \hat{B}(t_1) |\psi(0)\rangle \quad (25)$$

where  $\hat{B}(t) = \exp(-i\hat{H}_{\text{eff}}t/\hbar)$  describes the system evolution without jumps. Here,  $\hat{O}_n$  is the operator responsible

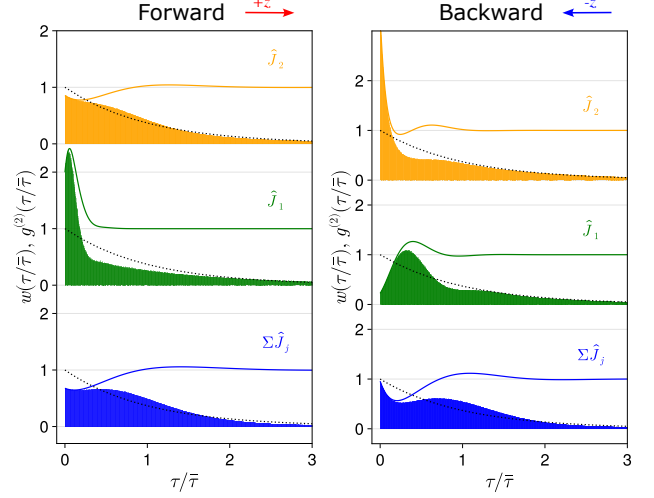


FIG. 3: Waiting time distributions and  $g^{(2)}(0)$  functions (solid lines) for individual source mode operators and all of them for forward and backward directions of excitation in a case of the two atom chain. The operators  $\hat{J}_j$  are sorted in the ascending order of corresponding decay rates, i.e.,  $\hat{J}_1$  corresponds to the dark state and  $\hat{J}_N$  corresponds to the bright state. The black dashed line shows the Poisson distribution of the waiting time.  $\bar{\tau}$  is the average waiting time for a corresponding operator. Parameters are the same as in Fig. 2(a, c)

for the  $n$ th jump, belonging to the set of jump operators  $\{\hat{O}_j\}$ .

The waiting time distribution (WTD) between photon emission events, which can be obtained from Monte Carlo simulations, provides valuable insight into the statistics of emission processes. Unlike coherence functions, which primarily provide information on intensity correlations, the WTD offers a more granular view of emission timings, revealing dynamic properties related to the system's collective and individual behaviors.

For example, in Fig. 3 and Fig. 4, we show the WTD and  $g^{(2)}(\tau)$  functions for source mode operators in two-atom and four-atom chains, respectively. These distributions illustrate that the WTD for a given operator or combination of operators is always less than or equal to the corresponding  $g^{(2)}$  function for the same operator(s). This trend highlights that while coherence functions indicate photon bunching or antibunching properties, the WTD can capture finer details about the collective nature of the emission events.

In Fig. 3, the WTDs reveal distinct temporal characteristics and correlations in the two-atom chain depending on the excitation direction.

In the *forward direction*, the WTD associated with the  $\hat{J}_1$  operator exhibits a sharp peak near  $\tau/\bar{\tau} = 0$ , indicative of strong photon bunching at short times. This sharp

feature suggests that  $\hat{J}_1$  contributes significantly to temporally correlated emissions immediately following excitation. In contrast, the WTD for  $\hat{J}_2$  starts close to 1 and gradually decays, reflecting weaker correlations and a lower tendency for bunching. The combined WTD for  $\sum \hat{J}_j$ , for jumps associated with any source-mode operator, starts below 1, indicating the absence of collective effects. Thus, forward excitation predominantly displays individual atomic emission characteristics, with  $\hat{J}_1$  as the primary source of temporal correlations, while  $\hat{J}_2$  displays uncorrelated emissions.

In the *backward direction*, both  $\hat{J}_1$  and  $\hat{J}_2$  show enhanced temporal correlations but with different time scales. The WTD for  $\hat{J}_2$  has a sharp peak near  $\tau/\bar{\tau} = 0$ , similar to that of  $\hat{J}_1$  in the forward case, indicating strong bunching at very short times.  $\hat{J}_1$ , however, exhibits a smaller, delayed peak, suggesting a distinct time scale of emission likely due to interference between atomic contributions. This delay introduces a second correlation peak and highlights the role of interference effects in shaping the emission dynamics. The combined WTD  $\sum \hat{J}_j$  in the backward direction shows a significantly higher peak at the initial time than in the forward case, indicating pronounced collective behavior. The enhanced WTD implies that, in the backward direction, photon emissions are strongly correlated in time, with both atoms contributing to collective bunching.

The direction-dependent WTDs illustrate that the backward excitation direction enhances collective effects through constructive interference, leading to pronounced bunching and temporal correlations. The observed peaks in the WTDs of  $\hat{J}_1$  and  $\hat{J}_2$  reveal how individual atomic contributions interact differently under directional excitation for the collective source modes, with backward excitation allowing for a more substantial interplay between the atomic operators.

Figure 4 presents the WTDs, and second-order correlation functions  $g^{(2)}(\tau)$  for a larger scale of an array, a four-atom chain, in both forward and backward directions, highlighting the influence of increased atom number on collective behavior compared to the two-atom case shown in Fig. 4. The collective source-mode operators  $\hat{J}_j$  are sorted by their decay rates, see eq. (8), with  $\hat{J}_1$  corresponding to the dark state and  $\hat{J}_N$  (here  $\hat{J}_4$ ) to the brightest state.

In the *backward direction*, the WTDs of  $\hat{J}_1$  and  $\hat{J}_2$  display features very close to Poisson distribution, which reflects the behavior of individual atoms. While the WTDs and  $g^{(2)}(\tau)$  of  $\hat{J}_1$  and  $\hat{J}_2$  demonstrate antibunching and bunching behaviour, respectively, the combined WTD for  $\sum \hat{J}_j$  shows individual behavior, close to Poisson distribution, similar to that observed in the two-atom case, see Fig. 3.

Similar to WTDs observed in the forward two-atom case, with  $\hat{J}_1$  showing a strong initial peak indicating photon bunching and  $\hat{J}_2$  displaying weaker correlations,

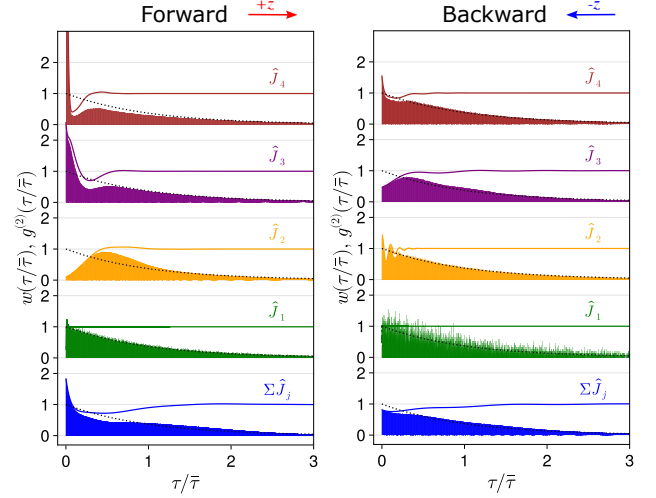


FIG. 4: Waiting time distributions and  $g^{(2)}(0)$  functions (solid lines) for individual source mode operators and all of them for forward and backward directions of excitation in a case of the four atom chain. The operators  $\hat{J}_j$  are sorted in the ascending order of corresponding decay rates, i.e.,  $\hat{J}_1$  corresponds to the dark state and  $\hat{J}_N$  corresponds to the bright state. The black dashed line shows the Poisson distribution of the waiting time. Parameters are the same as in Fig. 2(b, d)

the WTDs for  $\hat{J}_4$  and  $\hat{J}_3$  also demonstrate bunching and antibunching behavior, respectively. However, with four atoms, the WTDs for  $\hat{J}_3$  and  $\hat{J}_4$  introduce additional peaks, indicating the presence of more complex temporal correlations. The combined WTD for  $\sum \hat{J}_j$  now shows enhanced collective behavior, with contributions from multiple decay channels. This enhancement demonstrates that forward emission gradually incorporates a broader range of collective modes as the number of atoms increases, leading to more intricate emission dynamics.

The collective effects become more pronounced in the *forward direction*. The WTDs for each operator exhibit a clear separation of time scales, with  $\hat{J}_4$  and  $\hat{J}_3$  showing a prominent initial peak indicative of strong photon bunching, while  $\hat{J}_2$  and  $\hat{J}_1$  exhibit initial antibunching behavior and delayed correlations, but at different time scales. The forward combined WTD  $\sum \hat{J}_j$  shows a pronounced peak, underscoring a strong collective effect at the initial times. This peak is sharper and more sustained than in the two-atom case, indicating that constructive interference between atomic emissions becomes more substantial with additional atoms.

Overall, the comparison with a two-atom case, Fig. 3, reveals that increasing the number of atoms amplifies collective behavior. The separation of decay channels by their WTDs reflects enhanced temporal correlations and complex interference effects, key signatures of collective

emission in larger atomic chains.

Interestingly, the direction of excitation here plays a crucial role in determining the collective properties of the system. For one excitation direction, the system is trapped mostly in a collective state, demonstrating collective behavior in emission. A non-collective state is occupied in another direction of excitation, revealing the sum of emissions from individual atoms. For example, when excitation propagates in the backward direction in a two-atom chain (see Fig. 3), we observe enhanced collective behavior, with both WTD,  $w(\tau)$ , and  $g^{(2)}(\tau)$  values exceeding unity, consistent with previous findings [38]. Conversely, forward-directed excitation primarily exhibits individual atomic dynamics. This contrast becomes more pronounced as the number of atoms in the chain increases (see Fig. 4 for the four-atom case), where the forward direction emphasizes collective emissions. In contrast, the backward direction reinforces individual atomic contributions.

The WTD analysis of each source mode operator also sheds light on the interplay between the collective and individual dynamics of the atoms. This approach allows us to conclude that by merely switching the direction of excitation, we can toggle between regimes of individual atomic behavior and collective dynamics, at the same time significantly changing the angular pattern of the second-order coherence function,  $g^{(2)}$ , see Fig. 2.

## CONCLUSION

In this work, we have investigated the directional control of collective emission phenomena in atomic chains placed in free space. Our approach utilized theoretical modelling, and Monte Carlo simulations to analyze the emission statistics with the help of second-order correlation functions  $g^{(2)}(\tau)$ , WTDs,  $w(\tau)$ , for collective jump operators direction collective operators, focusing on how the direction of excitation influences temporal and spatial correlations in photon emissions.

The analysis began with the derivation of source-mode operators, enabling a detailed examination of collective states and their emission properties with the help of directional collective operators,  $\hat{S}(\theta, \varphi)$ , eq. (18). We showed that the  $g^{(2)}(\tau)$  function reveals asymmetries in photon statistics depending on whether the excitation is in the forward or backward direction. Specifically, we observed that backward excitation in a two-atom chain induces collective behavior, while forward excitation in a four-atom chain leads to a similar collective emission pattern. These results demonstrate that the emergence of collective behavior can be direction-dependent and can be further tuned by adjusting system parameters, such as atomic spin orientation, array geometry or transition frequencies of the atoms, allowing control over which direction excites a collective state.

The WTD analysis provided complementary insights into the temporal structure of emissions. For backward excitation in two-atom arrays, the emission shows pronounced photon bunching. In contrast, forward excitation in four-atom arrays also leads to bunched emission from the array, enhancing collective behaviour and more complex timing correlations. This directional dependence suggests that, by manipulating the direction of the excitation, one can switch between individual and collective atomic emissions, effectively controlling the temporal and spatial correlation properties of emitted photons.

Our study demonstrates a high degree of control over the collective behavior and angular emission statistics of atomic arrays by directing external excitation signals. By adjusting parameters such as spin orientation, array geometry and atomic transition frequencies, the emission characteristics — such as emission directionality and temporal correlations — can be finely tuned. This capability to externally modulate collective emission properties holds significant potential for applications in quantum optics, enabling the design of customizable photon sources with specific coherence and directional emission properties. Further exploration of larger arrays and complex configurations could provide additional insights into controllable light-matter interactions in free-space atomic ensembles.

This work has been partially supported by the Simons Foundation and the Air Force Office of Scientific Research MURI program.

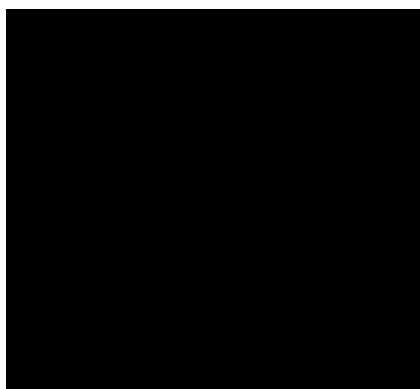
---

\* mnefedkin@gc.cuny.edu

† aalu@gc.cuny.edu

- [1] J. R. Friedman, V. Patel, W. Chen, S. Tolpygo, and J. E. Lukens, *nature* **406**, 43 (2000).
- [2] A. Mazurenko, C. S. Chiu, G. Ji, M. F. Parsons, M. Kanász-Nagy, R. Schmidt, F. Grusdt, E. Demler, D. Greif, and M. Greiner, *Nature* **545**, 462 (2017).
- [3] C. Gross and I. Bloch, *Science* **357**, 995 (2017).
- [4] S. Ebadi, T. T. Wang, H. Levine, A. Keesling, G. Semeghini, A. Omran, D. Bluvstein, R. Samajdar, H. Pichler, W. W. Ho, *et al.*, *Nature* **595**, 227 (2021).
- [5] R. Tao, M. Ammenwerth, F. Gyger, I. Bloch, and J. Zeiher, *Physical Review Letters* **133**, 013401 (2024).
- [6] F. Schäfer, T. Fukuhara, S. Sugawa, Y. Takasu, and Y. Takahashi, *Nature Reviews Physics* **2**, 411 (2020).
- [7] L. Amico, R. Fazio, A. Osterloh, and V. Vedral, *Reviews of modern physics* **80**, 517 (2008).
- [8] A. Asenjo-Garcia, M. Moreno-Cardoner, A. Albrecht, H. J. Kimble, and D. E. Chang, *Phys. Rev. X* **7**, 031024 (2017).
- [9] K. E. Ballantine and J. Ruostekoski, *PRX Quantum* **2**, 040362 (2021).
- [10] P.-O. Guimond, A. Grankin, D. V. Vasilyev, B. Vermer-sch, and P. Zoller, *Phys. Rev. Lett.* **122**, 093601 (2019).
- [11] R. H. Dicke, *Physical review* **93**, 99 (1954).

- [12] M. Gross and S. Haroche, Physics reports **93**, 301 (1982).
- [13] N. Nefedkin, E. Andrianov, A. Zyablovsky, A. Pukhov, A. Vinogradov, and A. Lisyansky, Optics Express **25**, 2790 (2017).
- [14] S. J. Masson, J. P. Covey, S. Will, and A. Asenjo-Garcia, PRX Quantum **5**, 010344 (2024).
- [15] N. Nefedkin, E. Andrianov, A. Zyablovsky, A. Pukhov, A. Dorofeenko, A. Vinogradov, and A. Lisyansky, Optics express **24**, 3464 (2016).
- [16] L. Mandel, *Optical Coherence and Quantum Optics* (Cambridge University Press, 1995).
- [17] B. Lounis and M. Orrit, Reports on Progress in Physics **68**, 1129 (2005).
- [18] M. Erhard, M. Krenn, and A. Zeilinger, Nature Reviews Physics **2**, 365 (2020).
- [19] J. L. O'brien, A. Furusawa, and J. Vučković, Nature Photonics **3**, 687 (2009).
- [20] C. Caloz, A. Alu, S. Tretyakov, D. Sounas, K. Achouri, and Z.-L. Deck-Léger, Physical Review Applied **10**, 047001 (2018).
- [21] H. Nassar, B. Yousefzadeh, R. Fleury, M. Ruzzene, A. Alù, C. Daraio, A. N. Norris, G. Huang, and M. R. Haberman, Nature Reviews Materials **5**, 667 (2020).
- [22] D. L. Sounas, J. Soric, and A. Alu, Nature Electronics **1**, 113 (2018).
- [23] A. R. Hamann, C. Müller, M. Jerger, M. Zanner, J. Combes, M. Pletyukhov, M. Weides, T. M. Stace, and A. Fedorov, Physical review letters **121**, 123601 (2018).
- [24] C. Müller, J. Combes, A. R. Hamann, A. Fedorov, and T. M. Stace, Physical Review A **96**, 053817 (2017).
- [25] N. Nefedkin, M. Cotrufo, A. Krasnok, and A. Alù, Advanced Quantum Technologies **5**, 2100112 (2022).
- [26] H. J. Carmichael, *Statistical methods in quantum optics 1: master equations and Fokker-Planck equations*, Vol. 1 (Springer Science & Business Media, 1999).
- [27] R. J. Bettles, M. D. Lee, S. A. Gardiner, and J. Ruostekoski, Commun Phys **3**, 141 (2020).
- [28] D. S. Wild, *Algorithms and Platforms for Quantum Science and Technology*, Ph.D. thesis, Harvard University (2020).
- [29] E. Shahmoon, D. S. Wild, M. D. Lukin, and S. F. Yelin, Phys. Rev. Lett. **118**, 113601 (2017).
- [30] S. Zhang, Y. Hu, G. Lin, Y. Niu, K. Xia, J. Gong, and S. Gong, Nature Photonics **12**, 744 (2018).
- [31] N. Nefedkin, M. Cotrufo, and A. Alù, Nanophotonics **12**, 589 (2023).
- [32] H. J. Carmichael and K. Kim, Optics communications **179**, 417 (2000).
- [33] J. Clemens, L. Horvath, B. Sanders, and H. Carmichael, Physical Review A **68**, 023809 (2003).
- [34] N. Nefedkin, E. Andrianov, A. Pukhov, and A. Vinogradov, Laser Physics **27**, 065201 (2017).
- [35] S. J. Masson, I. Ferrier-Barbut, L. A. Orozco, A. Browaeys, and A. Asenjo-Garcia, Phys. Rev. Lett. **125**, 263601 (2020).
- [36] J. D. Jackson, *Classical electrodynamics* (American Association of Physics Teachers, 1999).
- [37] H. J. Carmichael, *Statistical methods in quantum optics 2: Non-classical fields* (Springer Science & Business Media, 2009).
- [38] S. J. Masson and A. Asenjo-Garcia, Nature Communications **13**, 2285 (2022).

**Table of Contents**

ToC Entry